ISSN 1027-4510, Journal of Surface Investigation. X-ray, Synchrotron and Neutron Techniques, 2013, Vol. 7, No. 4, pp. 788–796. © Pleiades Publishing, Ltd., 2013.
Original Russian Text © A.E. Galashev, 2013, published in Poverkhnost'. Rentgenovskie, Sinkhrotronnye i Neitronnye Issledovaniya, 2013, No. 8, pp. 90–99.

Computer Study of the Spectral Characteristics and Structures of $(GaN)_{54}(SiO_2)_{50}$ Nanoparticles

A. E. Galashev

Institute of Industrial Ecology, Ural Branch, Russian Academy of Sciences, Yekaterinburg, 620219 Russia
e-mail: galashev@ecko.uran.ru

Received November 12, 2012

Abstract—The dielectric, structural, and kinetic properties of $(GaN)_{54}(SiO_2)_{50}$ nanoparticles of the following two types are studied using the method of molecular dynamics: particles of GaN covered by a SiO_2 layer and particles of SiO_2 with a GaN layer deposited onto it. The absorption and reflection spectra of these nanoparticles are considerably different in the respective frequency ranges $0 \le \omega \le 1500$ cm^{-1} and $\omega > 700$ cm^{-1}. The single-centered functions of the radial distribution of the nanoparticles differ in their peak positions and intensities, including the "tail" part for $r > 0.9$ nm. The structure of nanoparticles with the SiO_2 nucleus is completely tetrahedral, while the nearest six-atom environment is dominant in the structure of a particle with the GaN nucleus. The mobility of gallium atoms in the nanoparticles is lower by two orders than that of other elements constituting them.

DOI: 10.1134/S1027451013040319

INTRODUCTION

It is difficult to grow large GaN crystals using high-temperature methods [1] because of the thermal instability of the materials, which leads to their destruction before the instant of melting ($T_m \sim 2773$ K). As a result, GaN is mainly used in the form of thin films. Epitaxial GaN films play an important role in the development of photoelectronic devices such as diodes (blue/green ones) and laser diodes. The advantage of GaN is that it can produce effective luminescence even in the presence of a high density of crystal defects. This contradicts the general consensus that lattice defects behave as nonradiative recombination centers in semiconductors of the groups III–V. Recombination centers decrease the efficiency and the lifetimes of electronic devices. A lack of perfect substrates is the main reason hindering the progress of fabricating highly efficient GaN-based devices. Various single crystals (Al_2O_3, SiC, GaAs, and Si) have been intensively used as substrates for hetero-epitaxial GaN growth. Using the X-ray diffractometry method, the authors of [2] showed that it is possible to control the growth of GaN layers for small angles of disorientation of the crystallites forming these layers. Despite the large difference between the thermal expansion coefficients and lattice parameters of GaN and Si, an epitaxial GaN layer on a Si substrate is especially attractive for devices whose fabrication is being developed as a result of the integration of GaN into Si microelectronics.

The optical and electronic properties of GaN layers growing on both Si substrates and GaN crystals were studied in detail using Raman [4, 5] and infrared (IR) [6] spectroscopy. The structural and spectral properties of high-purity GaN films were studied using X-ray diffraction and Brillouin, Raman, and IR spectroscopy methods [7]. It was established that the moduli of elasticity C_{13} and C_{44} are more sensitive to residual stress than optical-phonon frequencies. The high-frequency ($\varepsilon_\infty = 5.14$) and static ($\varepsilon_0 = 9.04$) dielectric constants were determined. Short-wavelength devices are miniaturized using nanomaterials, including individual nanoparticles. Information on the properties of the nanomaterials of applied semiconductors is required in this case. Quartz (SiO_2) is a material suitable for the deposition of a GaN layer. The mechanism for the fixing of GaN onto a SiO_2 nanoparticle can be studied in computer experiments. The behavior of the $(SiO_2)_{325}$-nanoparticle surface tension under three-dimensional tensile strain was studied in [8]. The elastic properties and the stability of deformed Si nanoparticles were considered in [9, 10]. Interband radiative recombination can occur in Si nanocrystals with sizes of approximately 1 nm and is suppressed strongly in the Si bulk [11]. The optical properties of SiO_2 nanoparticles covered by GaN layers and of particles with inverse structures are, in fact, unknown.

The aim of this paper is to study the structural and kinetic properties of $(GaN)_{54}(SiO_2)_{50}$ nanoparticles of two types (a GaN particle covered by a SiO_2 layer and a SiO_2 particle with a GaN layer deposited onto it) and determine the frequency dependence of their complex permittivity and IR absorption and reflection spectra.

Table 1. Parameters of the optimized Tersoff potential

Parameter	Parameter*	Oxygen*	Gallium**	Nitrogen*
A, eV	1803.79	3331.06	993.88	6368.21
B, eV	471.195	260.476	136.123	511.205
λ_1, Å^{-1}	2.62392	3.78336	2.50842	5.60181
λ_2, Å^{-1}	1.88891	3.34402	1.49082	3.16170
R, Å	2.76581	2.78681	3.5	2.08389
D, Å	0.31772	0.52612	0.1	0.33133
b	1.0999×10^{-6}	1.00270	0.23586	4.4422×10^{-3}
n	0.78766	3.98638	3.47290	2.42635
h	–0.56239	–0.52909	0.71459	–0.52909
c	1.0039×10^{5}	0	0.07630	2.2955×10^{4}
d	16.21701	1	19.79647	24.78674
c	1	1	1	1

* The parameter values for Si, O, and N were obtained in [14], and ** those for Ga are taken from [15].

COMPUTER MODEL

The capability of the Tersoff-type potential is limited when describing distinctions between chemical interactions; however, it describes the chemical distinctions between the valence s and p electronic properties. This potential is an effective tool for modeling new materials. The Tersoff potential is based on the concept of bond order. The interatomic potential energy for two neighboring atoms i and j is written as [12]

$$V_{ij} = f_C(r_{ij})\left[Aa_{ij}\exp(-\lambda^{(1)}r_{ij}) - \chi Bb_{ij}\exp(-\lambda^{(2)}r_{ij})\right], \quad (1)$$

$$f_C(r_{ij}) = \begin{cases} 1, & r < R - D, \\ \frac{1}{2} - \frac{1}{2}\sin\left[\frac{\pi}{2}(r-R)/D\right], & R - D < r < R + D, \\ 0, & r > R + D, \end{cases} \quad (2)$$

where b_{ij} is the manyparticle bond-order parameter describing the creation of the bond formation energy (the attractive part of V_{ij}) for the local atomic position because of the presence of other neighboring atoms (k atoms). The potential energy is a manyparticle function of the positions of atoms i, j, and k and is determined by the following parameters:

$$b_{ij} = (1 + \xi_{ij}^{n_i})^{-1/(2n)}; \quad (3)$$

$$\xi_{ij} = \sum_{k\neq i,j} f_C(r_{ij})\beta_i g(\theta_{ijk})\exp\left[\lambda_3^3(r_{ij} - r_{ik})^3\right]; \quad (4)$$

$$g(\theta) = 1 + \frac{c^2}{d^2} - \frac{c^2}{\left[d^2 + (h - \cos\theta)^2\right]}; \quad (5)$$

$$a_{ij} = (1 + \alpha^n\eta_{ij}^{n_i})^{-1/(2n)}; \quad (6)$$

$$\eta_{ij} = \sum_{k\neq i,j} f_C(r_{ij})\exp\left[\lambda_3^3(r_{ij} - r_{ik})^3\right]; \quad (7)$$

$$\lambda_{ij}^{(k)} = (\lambda_i^{(k)} + \lambda_j^{(k)})/2, \quad A_{ij} = (A_iA_j)^{1/2}, \quad B_{ij} = (B_iB_j)^{1/2},$$
$$R^{(1)} = R - D, \quad R^{(2)} = R + D, \quad (8)$$
$$R_{ij}^{(1)} = (R_i^{(1)}R_j^{(1)})^{1/2}, \quad R_{ij}^{(2)} = (R_i^{(2)}R_j^{(2)})^{1/2},$$

where ξ is the effective coordination number, $g(\theta)$ is the function of the angle between r_{ij} and r_{ik}, which stabilizes the tetrahedral structure, and λ_3 and α are set to be zero.

The potential defined by expressions (1)–(7) differs from the corresponding potential for a one-component system [13] by the introduction of an additional parameter χ. This parameter increases or decreases the heteropolar bonds with respect to the value obtained by simple interpolation. Thus, the chemical interaction is included in this parameter or is incorporated when choosing the interpolation formula. Here, $\chi_{ii} = 1$ and $\chi_{ij} = \chi_{ji}$, so only one independent parameter is required for a pair of atoms of two types. The parameter β in (4) is included to achieve additional flexibility for a pair of atoms of different types.

The Tersoff-potential parameters for Si, O, Ga, and N are given in Table 1 [14, 15]. Optimized parameters are used in the potentials for Si, O, and N. The procedure chosen to optimize the potential parameters included simultaneous fitting of the energy and forces to the values obtained using calculations in accordance with density functional theory rather than traditional fitting of the potential to the physical properties [14]. The parameters $\lambda_{ij}^{(k)}$, A_{ij}, B_{ij}, and $R_{ij}^{(k)}$ of the

potential describing the interaction between atoms of the types i and j were calculated using arithmetic and geometric averages (of Eq. 8). The fitting procedure for the other parameters using the original Tersoff potential was given in [16]. The Tersoff potential can be used for bonding orbitals; the parameters fitted to the sp^3 hybridization can be used to describe interactions in materials with the sp^2 hybridization [17].

The initial configurations of the nanoparticles were created by cutting spheres and spherical layers from a GaN crystal with the wurtzite structure and from an α-quartz crystal and by the subsequent surrounding of the spheres with layers. The preliminarily created GaN crystal had the following lattice parameters: $a = b = 0.3181$ nm and $c = 0.5184$ nm [18]. The arrangement of the SiO_4 tetrahedrons to obtain an α-quartz crystal with the parameters $a = b = 0.5082$ nm and $c = 0.55278$ nm [19] was constructed using the GRINSP program-generator of inorganic crystalline structures [20]. To obtain the first-type nanoparticle, a GaN sphere was embedded into a spherical SiO_2 layer with the positions of their centers overlapping. The second-type nanoparticle was constructed similarly by fixing a SiO_2 sphere to a spherical GaN layer. In both cases, spherical-layer atoms located at distances to any sphere atoms that were less than a certain chosen value r_m were eliminated in the region including the sphere surface and the lower boundary of the spherical layer. As a result, after the nanoparticles were collected, the following minimum distances between atoms of the different types were obtained: 3.23 (Ga–Si), 2.67 (Ga–O), 2.22 (N–Si), and 2.00 Å (N–O). The sphere size was chosen so that it contained 50 SiO_2 structural units or 54 GaN atomic units. A similar number of structural units of each type were left in the external environment; atoms located furthest away from the center of mass of the created nanoparticle were eliminated in this case. The physical properties were calculated using a classical molecular-dynamics ensemble that was a particular case of the microcanonical ensemble. The equations of motion were integrated by the fourth-order Runge–Kutta method with the time step $\Delta t = 10^{-16}$ s. The atom velocities were corrected to balance the systems at a temperature of 300 K during the preliminary stage of calculation with a duration of $10^5\,\Delta t$. The main calculation was carried out without any correction and has a duration of $10^6\,\Delta t$. As a result, $T = 304.5$ K was established for the nanoparticle with the GaN nucleus, and $T = 303.3$ K, for the nanoparticle with the "inverse" structure.

INFRARED SPECTRA

The infrared spectra of the clusters can be calculated using the autocorrelation function of the total dipole moment. In the model, each atom can be regarded as a polarizable point dipole located at the atom nucleus. The interaction of the atom i having permanent polarizability $\alpha_{i,0}$ with neighboring atoms produces the induced dipole moment $\mathbf{d}_i$ [21]

$$\mathbf{d}_i = \mathbf{d}_{i,0} + \boldsymbol{\alpha}_{i,0}\sum_{j\neq i}\mathbf{T}_{ij}\mathbf{d}_j.$$

Here, $\mathbf{T}_{ij}$ is the dipole–dipole interaction tensor

$$\mathbf{T}_{ij} = \frac{1}{|r_{ij}|^3}\left(3\hat{\mathbf{r}}_{ij}\hat{\mathbf{r}}_{ij} - \mathbf{1}\right). \quad (9)$$

In Eq. (9), $\hat{\mathbf{r}}_{ij}$ is the unit vector in the direction $(\mathbf{r}_i - \mathbf{r}_j)$, where $\mathbf{r}_i$ and $\mathbf{r}_j$ are the positions of the nuclei of atoms i and j, and $\mathbf{1}$ denotes the unit (3×3) tensor. We used the following values for the atomic polarizability: 3.75 (Si), 0.793 (O), 8.1 (Ga), and 1.1 Å^3 (N) and the following values for the electric charges (in units of elementary electric charge): 4 (Si), –2 (O), 3 (Ga), and –3 (N) [22]. The standard iterative procedure [23] was used to calculate the induced dipole moments $\mathbf{d}_i$. The determination accuracy for $\mathbf{d}_i$ was given in the range 10^{-5}–10^{-4} D.

The static dielectric constant ε_0 was calculated via fluctuations of the total dipole moment $\mathbf{d}$ [24]:

$$\varepsilon_0 = 1 + \frac{4\pi}{3VkT}\left[\left\langle \mathbf{d}^2\right\rangle - \left\langle \mathbf{d}\right\rangle^2\right],$$

where V is the nanoparticle volume and k is the Boltzmann constant. The permittivity $\varepsilon(\omega)$ as a function of the frequency ω was represented by the complex quantity $\varepsilon(\omega) = \varepsilon'(\omega) - i\varepsilon''(\omega)$, the following equation was used to determine it [24, 25]:

$$\frac{\varepsilon(\omega) - 1}{\varepsilon_0 - 1} = -\int_0^\infty \exp(-i\omega t)\frac{dF}{dt}dt$$
$$= 1 - i\omega\int_0^\infty \exp(-i\omega t)F(t)dt,$$

where the function $F(t)$ is the normalized autocorrelation function of the total dipole moment of the nanoparticle:

$$F(t) = \frac{\left\langle \mathbf{d}(t)\cdot\mathbf{d}(0)\right\rangle}{\left\langle \mathbf{d}^2\right\rangle}.$$

The absorption cross section for IR radiation is defined as

$$\sigma(\omega) = \left(\frac{2}{\varepsilon_v c\hbar n}\right)\omega\,\mathrm{th}\left(\frac{\hbar\omega}{2kT}\right)$$
$$\times\,\mathrm{Re}\int_0^\infty dt\exp i\omega t\left\langle \mathbf{M}(t)\cdot\mathbf{M}(0)\right\rangle, \quad (11)$$

where n is the refraction coefficient, ε_v is the permittivity of vacuum, and c is the speed of light.

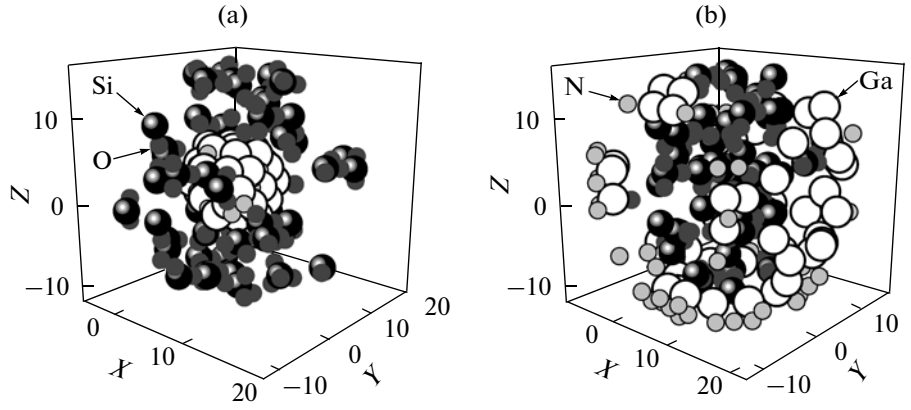

Fig. 1. Configuration of the $(GaN)_{54}(SiO_2)_{50}$ nanoparticles corresponding to a time instant of 100 ps; the nanoparticle nuclei are (a) GaN and (b) SiO_2.

The reflection coefficient R is defined as the ratio of the average energy flux reflected from the surface to the incident flux. In the case of normal incidence of the plane monochromatic wave, the reflection coefficient is given by the formula [26]

$$R = \left| \frac{\sqrt{|\varepsilon_1|} - \sqrt{|\varepsilon_2|}}{\sqrt{|\varepsilon_1|} + \sqrt{|\varepsilon_2|}} \right|^2 . \quad (12)$$

It is assumed here that the wave propagates from a transparent medium (medium 1) to the medium that can be transparent and nontransparent, i.e., the absorbing and scattering one (medium 2). The subscripts for the permittivity in expression (12) denote the medium.

RESULTS OF THE CALCULATION

The configurations of nanoparticles with GaN in the central region and at the periphery obtained at a time instant of 100 ps are shown in Fig. 1. The SiO_2 arrangement (especially for the external arrangement of these structural units in the nanoparticle) corresponds to the amorphous state to a greater extent than to α quartz. In both cases, individual O atoms escape from Si atoms and approach Ga atoms. In the case where GaN is located on the cluster surface, N atoms are tightly pressed against Ga atoms and do not penetrate into the cluster. Ga atoms can be in contact with Si and O atoms. The SiO_2 skeleton is retained except for some losses of O atoms. The inner SiO_2 nucleus has dense and sparse regions. Ga atoms adjoin this nucleus rather closely. If GaN is located in the central region of the nanoparticle, then the SiO_2 surface layer is strongly inhomogeneous and has ruptures. Only individual O atoms approach the GaN nucleus, coming into contact with Ga atoms. The GaN nucleus retains its sphere-like shape during the entire calculation. The N and Ga atoms are tightly bound to one another. During the calculation, these bonds are not broken. Moreover, N atoms tend enter inside the GaN nucleus. Figure 2 gives a more exact representation of atomic packing in the GaN nucleus. It can be seen that, on the whole, Ga and N atoms form alternating rows. Some rows of Ga and N atoms are greatly curved and are even broken. However, atoms of different types do not mix completely. Ga atoms mainly form the nucleus surface.

Figure 3 shows the real and imaginary parts of the $(GaN)_{54}(SiO_2)_{50}$ nanoparticle permittivity. The frequency dependences of ε' and ε'' of the nanoparticles with the nucleus of GaN and SiO_2 are significantly different. The functions ε'(ω) and ε''(ω) for the nanoparticle with the GaN nucleus have smoother forms. The maximum ε' is at a frequency of 1208 cm^{-1} for the particle with the GaN nucleus and at a frequency of 1240 cm^{-1} for the particle with the SiO_2 nucleus. In both cases, the minimum is observed near 1048 cm^{-1} at a nonzero frequency. The maximum value of the function ε''(ω) corresponds to a frequency of 1095 cm^{-1}

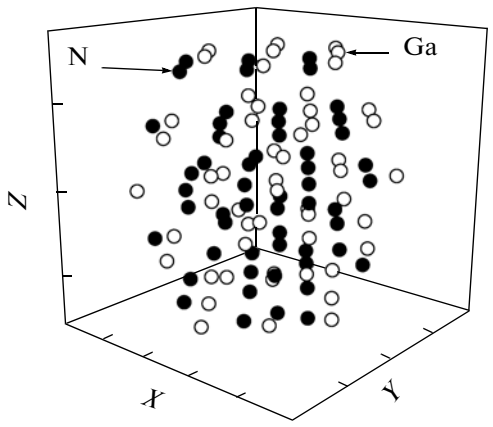

Fig. 2. Configuration of the nanoparticle GaN nucleus that corresponds to a time instant of 100 ps.

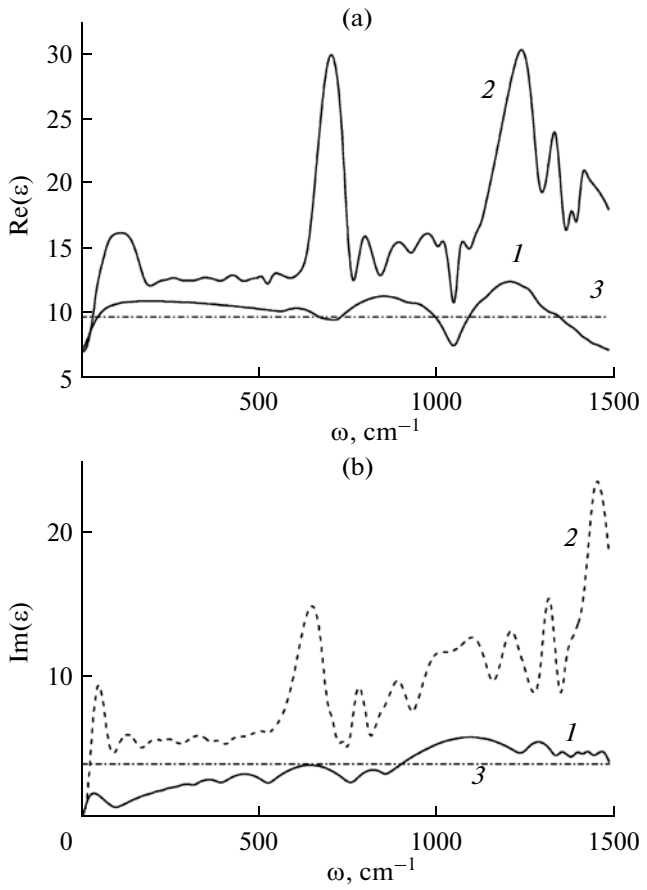

Fig. 3. (a) Real and (b) imaginary parts of the permittivity of the $(GaN)_{54}(SiO_2)_{50}$ nanoparticles with a nuclei formed of (*1*) GaN and (*2*) SiO_2; (*3*) the experimental static dielectric permittivity: (a) GaN and (b) SiO_2.

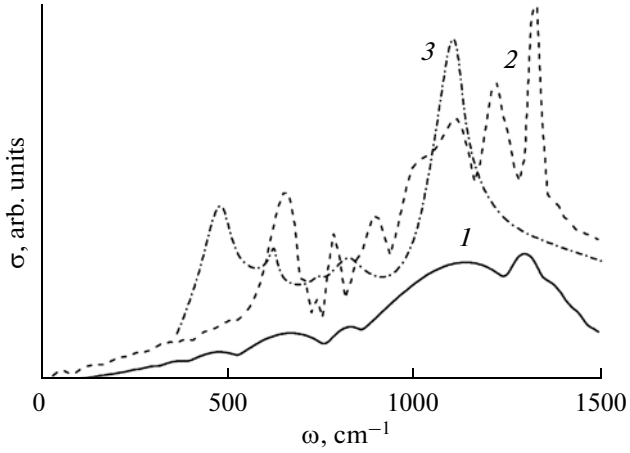

Fig. 4. Infrared absorption spectra for the $(GaN)_{54}(SiO_2)_{50}$ nanoparticles with a nuclei formed from (*1*) GaN and (*2*) SiO_2; (*3*) IR absorption spectrum for the $GaN/SiO_2/Si$ nanocrystals with an average size of $h = 50$ nm [27].

for the nanoparticle with the GaN nucleus and to 1449 cm^{-1} for the particle whose central region is formed by SiO_2. The minimum of this function for a nonzero frequency is at 91 cm^{-1} for the first-type particle and at 85 cm^{-1} for the second-type particle. The static permittivities of the bulk GaN and SiO_2 are shown in Figs. 3a and 3b by the straight dashed lines. Knowing the frequency dependence of the complex permittivity makes it possible to determine a series of dielectric properties.

The IR absorption spectra of the $(GaN)_{54}(SiO_2)_{50}$ nanoparticles are shown in Fig. 4 (curves *1* and *2*). The spectrum $\sigma(\omega)$ of the nanoparticle with the SiO_2 nucleus is characterized by several well-resolved peaks, while the particle with the GaN nucleus has a rather smooth frequency spectrum $\sigma(\omega)$, in which a series of modes can also be singled out. The IR radiation absorption spectrum of the nanoparticle whose internal part consists of SiO_2 is characterized by lines with higher intensities. For comparison, this figure also shows the experimental IR absorption spectrum of a GaN film grown on a SiO_2/Si substrate [27]. Such a structure is of considerable interest for the development of devices based on the integration of GaN into Si microelectronics. The experimental IR absorption spectrum for the GaN nucleus with island heights of $h = 50$ nm has intense bands at 480 and 1100 cm^{-1}, which are due to the presence of Si atoms [6]. A series of bands at 472, 680, 824, 1128, and 1289 cm^{-1} are observed in the IR spectrum of the $(GaN)_{54}(SiO_2)_{50}$ nanoparticle with the GaN nucleus. The majority of them are, probably, due to the superposition of closely located absorption signals. The low-intensity bands at 680 and 824 cm^{-1} can be compared with the bands of the experimental IR spectrum of α quartz: 685 and 789 cm^{-1}, and the strong band at 1128 cm^{-1}, with the high-intensity band of α quartz at 1063 cm^{-1} [28]. When going from bulk α quartz to silica gel, the asymmetric transverse optical mode (1063 cm^{-1}) shifts to the frequencies 1100, 1150, 1140, and 1120 cm^{-1} for 3-, 4-, 5-, and 6-link rings of SiO_2, respectively [29]. A change in the silica-gel density from 1 to 2 g/cm^3 shifts this band from 1078 to 1122 cm^{-1}. The mode localization also varies strongly with temperature. The band at 1289 cm^{-1} can be compared with the asymmetric valence mode (1200 cm^{-1}) in silica-gel glass [30]. This mode belonging to optically active oxygen and describing asymmetric stretching was experimentally observed for thin films of amorphous SiO_2 in the form of peaks in the range 1076–1256 cm^{-1}. Bands at 651, 781, 889, 1107, 1212, and 1313 cm^{-1} are pronounced in the IR spectrum of the nanoparticle with the SiO_2 nucleus. The first, second, and fourth bands can be regarded as bands corresponding to α quartz. However, it can also be assumed that the fourth band is due

to the presence of GaN. It is likely that the last two bands are caused by the interaction between the GaN and SiO_2 subsystems.

The calculated reflection spectra of $(GaN)_{54}(SiO_2)_{50}$ nanoparticles with GaN and SiO_2 nuclei differ considerably from one another, because the surface structures are different (Fig. 5). The spectrum $R(\omega)$ for the particle with the GaN nucleus is characterized by high intensities in the frequency range $\omega > 687$ cm^{-1}. The minimum of the function $R(\omega)$ is observed at a frequency of 687 cm^{-1}. The frequency 1176 cm^{-1} corresponds to the maximum of the function $R(\omega)$. The deepest minimum in the dependence $R(\omega)$ for the nanoparticle with the SiO_2 nucleus is at a frequency of 1052 cm^{-1}, and the most intense band of this spectrum corresponds to a frequency of 1329 cm^{-1}. The Ga and N polar faces of the GaN crystal with the wurtzite structure suggest a difference between their adsorption and optical properties. Hydride epitaxy in the vapor phase was performed on the Ga and N polar faces of the GaN single crystal at high pressure [31]. The GaN films had layered atomic structures. The IR reflection spectra of the GaN films grown on the Ga and N polar sides differ considerably from one another. The spectrum for the N polar layer turned out to be dominant because of reflection from a free-electron plasma. The IR reflection spectrum for the Ga polar layer had an intense band produced by a longitudinal phonon in the range 500–750 cm^{-1}. Curve *3* in Fig. 5 corresponds to the combined IR reflection spectrum obtained in the form of the arithmetical mean of the corresponding spectra related to the Ga and N sides of the GaN crystal. This spectrum has one broad intense band in the vicinity of the frequency 663 cm^{-1}. Weakly pronounced bands at 564 (the GaN nucleus) and 614 cm^{-1} (the SiO_2 nucleus) are the nearest ones to it. The silica-gel reflection spectrum has a high-intensity band at 1084 cm^{-1} [29] (Fig. 5, curve *4*). Thus, when transitioning from a crystalline structure to an amorphous one, the most intense band in the reflection spectrum shifts to the blue spectral region and approaches the positions of intense bands in the reflection spectrum of $(GaN)_{54}(SiO_2)_{50}$ nanoparticles.

The traditional structural characteristic of a physical system is the radial distribution function $g(r)$. This one-dimensional function determines a spherically averaged structure rather than reflects the total pattern of the spatial structure. In a series of cases, a conclusion regarding the physical state of the system can be drawn if the shape of this function is used. The distances between the nearest neighbors and the peak intensities of $g(r)$ are important parameters. The functions $g(r)$ constructed around the atom nearest to the center of mass of the $(GaN)_{54}(SiO_2)_{50}$ nanoparticles

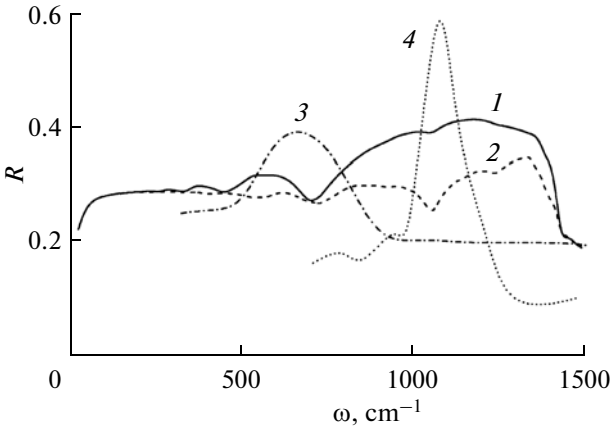

Fig. 5. Infrared reflection spectra for the $(GaN)_{54}(SiO_2)_{50}$ nanoparticles with a nuclei formed from (*1*) GaN and (*2*) SiO_2; (*3*) IR reflection spectrum obtained by averaging the corresponding spectra for the N and Ga polar layers grown by the method of hydride vapor-phase epitaxy [31]; and (*4*) the reflection spectrum for silica-gel glass at $T = 453$ K [30].

are shown in Fig. 6 (curves *1*). The function $g(r)$ calculated for the atom nearest to the center of mass of the $(GaN)_{129}$ nanoparticle is shown in the inset in Fig. 6a, and a similar function for the $(SiO_2)_{86}$ nanoparticle is shown in the inset in Fig. 6b. The arrows indicate the peak positions in nanometers. On the one hand, the majority of sharp $g(r)$ peaks of the $(GaN)_{54}(SiO_2)_{50}$ nanoparticles, including allowed ones, demonstrate that the system state can be regarded as the crystalline one. On the other hand, the majority of peaks are not fully resolved, which is evidence of the fragmentary destruction of the crystalline order. For the nanoparticle with the GaN nucleus, the first peak is localized at 0.163 nm and the second, one at 0.407 nm. The peaks of the function $g(r)$ of the $(GaN)_{129}$ nanoparticle at 0.244 and 0.353 nm disappear in this case. For the radial distribution function of the particle with the SiO_2 nucleus, all peaks of the function $g(r)$ of the $(SiO_2)_{86}$ nanoparticle are reproduced up to a distance of ~0.9 nm; the first of them is at 0.162 nm. The "tail" parts of the functions $g(r)$ (for $r > 0.9$ nm) for particles with the GaN and SiO_2 nuclei are characterized by different peaks, which are evidence of the existence of noncrystalline structure at the periphery for the first nanoparticle and of the crystalline type of periphery ordering for the second particle. The periphery of the first particle is mainly represented by SiO_2, and that of the second particle, by GaN. Curves *2* in Fig. 6 correspond to the experimental functions $g(r)$ for the GaN nanocrystal [18] with an average size of ~10 nm (Fig. 6a) and for glass SiO_2 (Fig. 6b) [32]. The radial distribution function for the GaN nanocrystal has many peaks; they disappear at considerably smaller

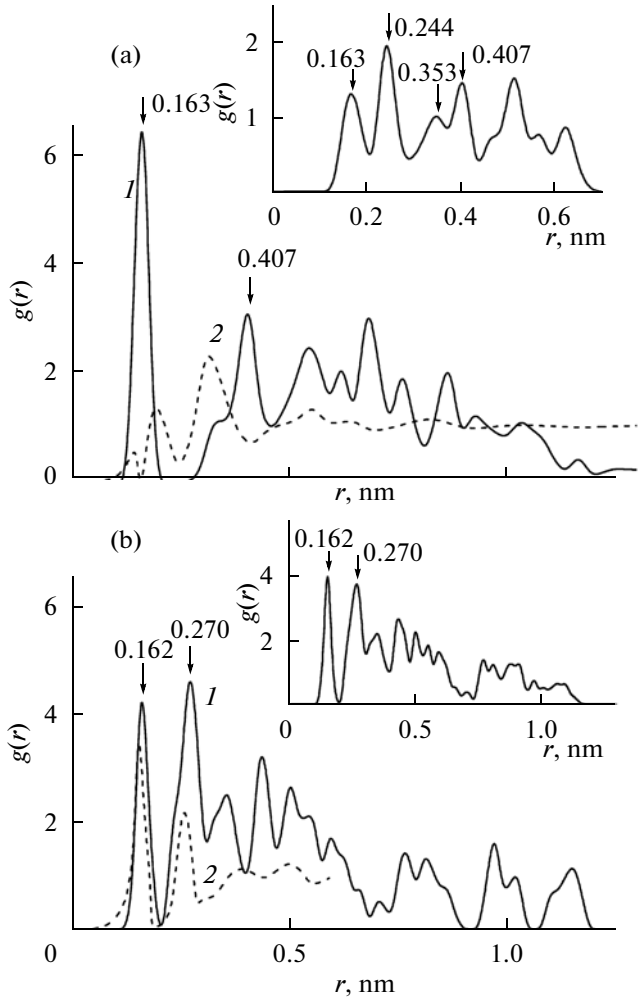

Fig. 6. (*1*) Radial distribution functions for the $(GaN)_{54}(SiO_2)_{50}$ nanoparticles with nuclei formed from (*1*) GaN and (*2*) SiO_2; (*2*): (a) the function $g(r)$ of the GaN nanocrystals with an average size of ~10 nm (experiments in [18]) and (b) the function $g(r)$ for SiO_2 glass (experiments in [32]); the insets shows $g(r)$ of (a) the $(GaN)_{129}$ and (b) the $(SiO_2)_{86}$ nanoparticles.

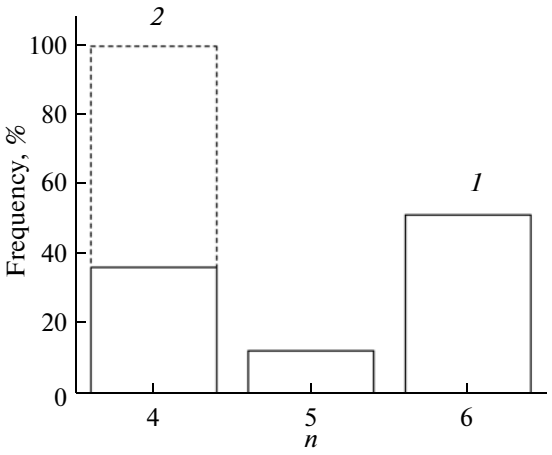

Fig. 7. Distribution of the VP faces for $(GaN)_{54}(SiO_2)_{50}$ nanoparticles with nuclei formed from (*1*) GaN and (*2*) SiO_2.

distances than peaks of the function $g(r)$ for crystalline GaN. Consequently, nanocrystalline GaN loses its long-range order, which ordinary crystals of this compound have. The first peak for the nanocrystal is small, and its position corresponds approximately to 0.14 nm. This peak is fully attributed to bound N–N pairs. The second peak is located at 0.194 nm. This value is the average distance between the first Ga–N neighbors. The third peak is located at approximately 0.316 nm. It mainly reflects the Ga–Ga neighborhood and, to a lesser extent, the N–N distances. The GaN nanoparticle under study covered by the SiO_2 layer had an average size of ~2.8 nm. Obviously, the SiO_2 film had a certain influence on the structure of the GaN nucleus of this particle. This is demonstrated by a significant increase in the first-peak intensity of the function $g(r)$ and also by the disappearance of the peaks at 0.244 and 0.353 nm. The positions of the first (0.162 nm) and second (0.265 nm) peak for glass SiO_2 reflect the average nearest Si–O and O–O distances. The two first peaks are located at 0.162 and 0.270 nm for the nanoparticle with the SiO_2 nucleus under study. Based on the form of the function $g(r)$, we can conclude that the nanoparticle-nucleus structure turns out to be very similar to the structure of a free $(SiO_2)_{86}$ nanoparticle. We note that, unlike the experimental function $g(r)$, the calculated radial distribution functions reflect only the local nanoparticle structure.

The method of statistical geometry based on constructing Voronoi polyhedrons (VP) determines the spatial structure more precisely. A VP includes a spatial part all points of which are located closer to the center of the polyhedron under study than to other atomic nuclei. To construct a VP, it is necessary that any plane passing through its center divides the space into two parts, so that at least one atom can be located in each half-space. Obviously, a polyhedron cannot be constructed for individual atoms located on the nanoparticle surface. Therefore, the VPs were constructed not for 254 atoms, but for only 200 atoms located closer to the center of the nanoparticle mass; therefore, the statistics represented by the polyhedrons reflects the structure of the nanoparticle interior to a larger extent. The VP distribution over the number of faces shows the average statistical arrangement of the nearest geometric neighbors. The number of nearest neighbors is always four in the case of the nanoparticle with the GaN nucleus, and four–six neighbors can be located in the nearest environment of the nanoparticle with the SiO_2 nucleus; in this case, the presence of six neighbors occurs in half of the cases or more (Fig. 7). The distributions shown in Fig. 7 are constructed based on an analysis of 200000 polyhedrons. The VPs

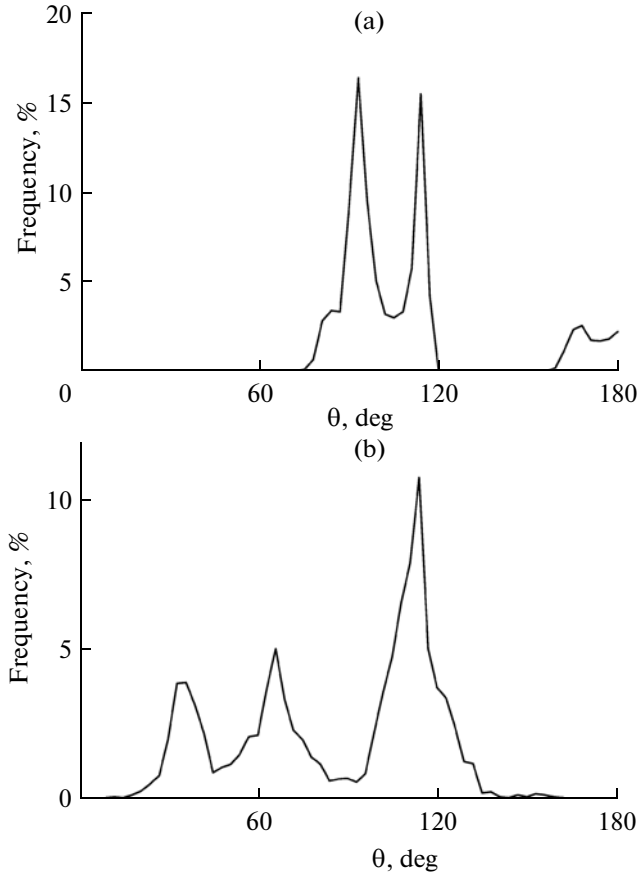

Fig. 8. Angular distribution of the nearest geometric neighbors for $(GaN)_{54}(SiO_2)_{50}$ nanoparticles with nuclei formed from (*1*) GaN and (*2*) SiO_2.

were constructed using the atom coordinates recorded after every 1000 time steps.

To construct the angular distribution of the nearest geometric neighbors, we considered the angles θ with vertices in the nuclei of VP atom-centers and sides formed by lines passing through these vertices and the nuclei of atoms forming the VP faces. The θ distributions for $(GaN)_{54}(SiO_2)_{50}$ nanoparticles shown in Fig. 8 have three peaks. In the case of the nanoparticle with the GaN nucleus, these peaks are at 93°, 114°, and 168°, and, in the case of the nanoparticle with the SiO_2 nucleus, the peaks are at 35°, 66°, and 114°. The angle 66° is a supplement to the angle 114°, because the addition of these angles gives the straight angle: 66° + 114° = 180°. The angle 114° corresponds to the maximum stability of the structural elements Si–O–Si with one single bond and one double bond in which the O atom participates [33]. The peak at small angles 35° is indicative of the elongated form of the polyhedrons, which follows from the fixing of the interatomic distances. In turn, the presence of elongated VPs indicates the structural inhomogeneity of the obtained nanoparticles.

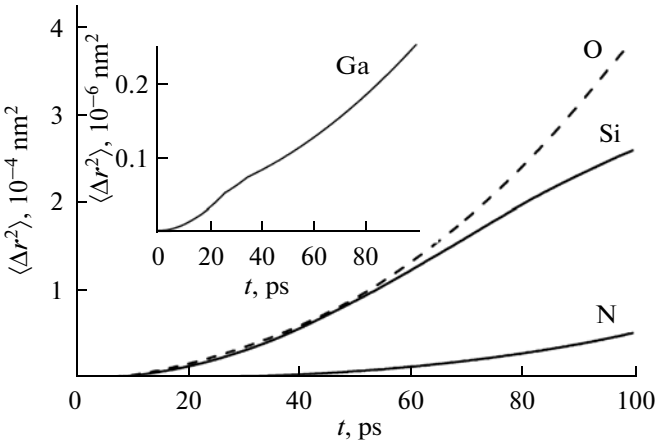

Fig. 9. Average squared atomic displacement in the $(GaN)_{54}(SiO_2)_{50}$ nanoparticle with a nucleus formed from SiO_2.

The character of atomic motion in the nanoparticles was determined calculating the average squared displacement of atoms $\langle (\Delta r)^2 \rangle$. Figure 9 shows the dependences $\langle (\Delta r)^2 \rangle (t)$ for Ga, N, Si, and O atoms in the nanoparticle with the SiO_2 nucleus. Similar dependences were obtained for the nanoparticle whose nucleus consists of GaN. The value of the atomic displacement in the nanoparticle was determined not only by their mass, but also by the local density, i.e., the character of the nearest environment. An estimate of the GaN density is 6.15 g/cm^3, and the α-quartz density is 2.65 g/cm^3 [20]. Consequently, it can be expected that the atomic displacement in GaN is noticeably smaller than in SiO_2. The mass of the Ga atom is five times larger than that of the N atom. Therefore, the N atoms must have a higher mobility. The mass of the Si atom exceeds that of the O atom by a factor of 1.75. As a consequence, the mobility of O atoms must be noticeably higher. The self-diffusion coefficients D in the $(GaN)_{54}(SiO_2)_{50}$ nanoparticles, which were determined using the average squared displacement, are given in Table 2. It can be seen that the coefficient D of N atoms is larger than that for Ga atoms by a factor of 160.7. At the same time, the coefficient D of the O atoms is larger than that for the Si

Table 2. Self-diffusion coefficients for $(GaN)_{54}(SiO_2)_{50}$ nanoparticles

	Ga	N	Si	O
D, 10^{-12} m^2/s	0.00729	1.172	2.956	7.746

atoms by a factor of 2.6. The mobility of the O atoms is higher than that for the N atoms by a factor of 6.6.

CONCLUSIONS

The complex interatomic interactions in $(GaN)_{54}(SiO_2)_{50}$ nanoparticles were described by the Tersoff potential with parameters optimized using density functional theory. N atoms have a significantly higher mobility than Ga atoms. However, the GaN–SiO_2 interaction occurs mainly by means of Ga atoms. The frequency dependence of the real and imaginary parts of the permittivity and the IR absorption spectra of the $(GaN)_{54}(SiO_2)_{50}$ nanoparticles are rather smooth if there is GaN at the particle nucleus and have an oscillatory character in the presence of SiO_2 at the nucleus. The IR absorption spectra of the nanoparticles under study contain a broad intense absorption band in the frequency range $850 \le \omega \le 1350$ cm^{-1}. As the frequency increases, the reflection coefficient of the IR radiation of the nanoparticle with the GaN nucleus becomes noticeably larger than that of the nanoparticle with the SiO_2 nucleus, starting from a frequency of 750 cm^{-1}. The radial distribution functions of the nanoparticles with the GaN and SiO_2 nuclei are significantly different. For the first-type nanoparticle, the first peak of the function $g(r)$ is resolved and has a high intensity. For the second-type nanoparticle, the second-peak intensity of this function exceeds the intensity of the first peak. In addition, the "tail" parts of the function $g(r)$ of the nanoparticles under study have different shapes, positions, and peak intensities. The tetrahedral structure of the nanoparticle is retained during the entire calculation if its nucleus is SiO_2. The structure becomes predominantly of the six-coordinate type if the nanoparticle nucleus is GaN. The angular distribution of the nearest geometric neighbors is characterized by two strong peaks at angles of 93° and 114° for the nanoparticle with the GaN nucleus and by one peak with a high intensity localized at 114° for the nanoparticle with the SiO_2 nucleus. The self-diffusion coefficients calculated using the average squared atomic displacements have the following sequence: Ga, N, Si, and O in ascending order of D. In this case, Ga is characterized by the a-diffusion coefficient that is lower by two orders than those of the other elements in the $(GaN)_{54}(SiO_2)_{50}$ nanoparticle.

ACKNOWLEDGMENTS

This work was supported by the Presidium of the Ural and Far Eastern Branches of the Russian Academy of Sciences (integration project no. 09-C-2-1004).

REFERENCES

1. M. Bockowski, Cryst. Res. Technol. **36**, 771 (2001).
2. Yu. N. Drozdov, M. N. Drozdov, O. I. Khrykin, and V. I. Shashkin, J. Surf. Invest. **4**, 998 (2010).
3. M. Benyonul, M. Kuball, B. Benumont, and P. Gibart, Appl. Phys. Lett. **80**, 2275 (2002).
4. G. S. Cheng, L. D. Zhang, Y. Zhou, et al., Appl. Phys. Lett. **75**, 2455 (1999).
5. Y. G. Cao, X. L. Chen, Y. C. Lan, et al., J. Mater. Res. **15**, 267 (2000).
6. X. Zhang, Y. T. Hou, Z. C. Feng, and J. L. Chen, J. Appl. Phys. **89**, 6165 (2001).
7. T. Deguchi, D. Ichiryu, K. Toshikawa, et al., J. Appl. Phys. **86**, 1860 (1999).
8. A. E. Galashev, Poverkhnost', No. 8, 95 (2010).
9. A. E. Galashev, V. A. Polukhin, I. A. Izmodenov, and O. A. Galasheva, Poverkhnost', No. 10, 60 (2007).
10. A. E. Galashev, I. A. Izmodenov, O. R. Rakhmanova, and O. A. Novruzova, Poverkhnost', No. 8, 95 (2007).
11. V. A. Belyakov, V. A. Burdov, and K. V. Sidorenko, J. Surf. Invest. **4**, 987 (2010).
12. J. Tersoff, Phys. Rev. B **39**, 5566 (1989).
13. J. Tersoff, Phys. Rev. Lett. **56**, 632 (1986).
14. S. R. Billeter, A. Curioni, D. Fischer, and W. Andreoni, Phys. Rev. B **73**, 155329 (2006).
15. Y. Nishidate and G. P. Nikishkov, Comp. Model. Eng. Sci. **26**, 91 (2008).
16. A. Yasukawa, Jpn. Soc. Mech. Eng. **39**, 313 (1996).
17. F. Benkabou, M. Certier, and H. Aourag, Mol. Simul. **29**, 2001 (2003).
18. V. Petkov, M. Gateshki, J. Choi, et al., J. Mater. Chem. **15**, 4654 (2005).
19. S. Munetoh, T. Motooka, K. Moriguchi, and A. Shintani, Comp. Mater. Sci. **39**, 334 (2007).
20. A. le Bail, J. Appl. Crystallogr. **38**, 389 (2005).
21. W. B. Bosma, L. E. Fried, and S. Mukamel, J. Chem. Phys. **98**, 4413 (1993).
22. *The Chemist's Guide*, Ed. by B. P. Nikol'skii (Khimiya, Leningrad, 1971), Vol. 1 [in Russian].
23. L. X. Dang and T.-M. Chang, J. Chem. Phys. **106**, 8149 (1997).
24. F. Bresme, J. Chem. Phys. **115**, 7564 (2001).
25. M. Neumann, J. Chem. Phys. **82**, 5663 (1985).
26. L. D. Landau and E. M. Lifshits, *Course of Theoretical Physics*, Vol. 8: *Electrodynamics of Continuous Media* (Nauka, Moscow, 1982; Pergamon, New York, 1984).
27. V. N. Bessolov, Yu. V. Zhilyaev, E. V. Konenkova, et al., Semiconductors **37**, 940 (2003).
28. Y. Liang, C. R. Miranda, and S. Scandolo, J. Chem. Phys. **125**, 194524 (2006).
29. J. K. West, D. J. West, and L. L. Hench, Phys. Chem. Glass **39**, 314 (1998).
30. C. T. Kirk, Phys. Rev. B **38**, 1255 (1988).
31. F. Tuomisto, T. Suski, H. Teisseyre, et al., Phys. Status Solidi B **240**, 289 (2003).
32. P. A. V. Johnson, A. C. Wright, and R. N. Sinclair, J. Non-Cryst. Solids **58**, 109 (1983).
33. L. Pauling, Am. Mineral. **65**, 321 (1980).

Translated by L. Kul'man